Impact Failure of Poly(methyl Methacrylate)

L. BEVAN* and P. E. REED

Department of Materials, Queen Mary and Westfield College, Mile End Road, London E1 4NS, United Kingdom

SYNOPSIS

Damage development during instrumented falling weight impact (IFWIM) testing of poly(methyl methacrylate) (PMMA) is recorded using short pulse photography. The first visible damage is cracking on application of the peak force. Finite element analysis predicts the deformation and state of stress throughout the specimen until the first point of failure is reached. A variation in the specimen geometry produces a significant change in initial failure energy, while the maximum tensile stress is approximately constant. The proposed failure criterion is the attainment of a critical time-dependent value of tensile stress.

INTRODUCTION

The instrumented flexed plate impact test is, as currently performed and interpreted, essentially a component test, in which forces and energies are estimated at prescribed and selected positions, especially at the peak, on the measured force–time or force–displacement curve. Forces and energies so determined are dependent on the material tested, but they are not true material properties since they are very dependent on the geometry of the specimen and of the test configuration. This investigation places emphasis on the stress state in order to determine if the maximum tensile stress at damage initiation is material property rather than a geometry-dependent parameter.

The required stress analysis may be carried out using a closed form linear-elastic solution, which Reed[1] derived for the flexed plate problem. The applied central force is modelled as a circular line load at a small radius, which must be assumed. In this article, the finite element method, which Nimmer[2] used in the elastic–plastic analysis of the drop-weight impact of a polycarbonate disc, is used to model the contact between the impactor and the plate and to estimate the stresses both within and outside the central zone.

* To whom correspondence should be addressed.

Journal of Applied Polymer Science, Vol. 46, 2131–2137 (1992)
 CCC 0021-8995/92/122131-07

EXPERIMENTATION AND COMPUTATION

Tests are conducted at room temperature, 20°C, using a CEAST instrumented falling weight tester with a 20 mm diameter hemispherical striker and an impact velocity of 4.43 m/s. Square specimens, 60 mm × 60 mm, 100 mm × 100 mm, and 140 mm × 140 mm, are cut from the same 3 mm thick sheet of PMMA (ICI Perspex) and they are supported, unclamped, on circular rings of 40 mm, 80 mm, and 120 mm diameter, respectively. Force–time traces are obtained and short-pulse photography is used to monitor damage at various stages in the impact test. The camera is mounted below the plate and the photographic background is provided by positioning a sheet of white paper, with a central hole of greater area than the projected area of the striker, above the plate.

The finite element analysis is an axisymmetric one, using the code ABAQUS. Axial symmetry applies to the striker and the major portion of the plate, that is, from the center to the supports. The fact that the supported portion of the plate is not annular has a negligible effect on the calculated maximum stress, which occurs at the center of the plate. The striker is modeled as a rigid body and interface elements are used to represent contact between the striker and the plate. The mesh, of 8-noded elements, for the 60 mm plate is shown in Figure 1. The idealization of the other plates is similar and in all cases the mesh is refined in the region of the

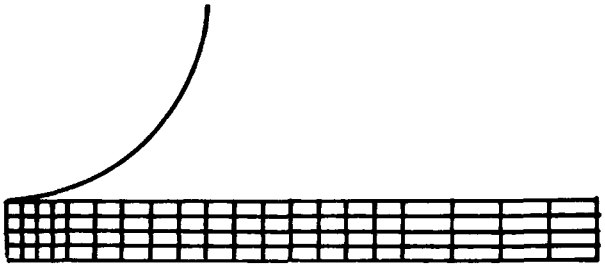

Figure 1 Finite element mesh for the 60 mm square plate.

plate center, the radius of the region being taken as equal to the plate thickness. When crack propagation occurs, axial symmetry is not preserved, but this does not affect the present analysis, which considers the initiation of damage and is, therefore, based on the peak load. The analysis is essentially a pseudoelastic one, in which the material modulus is changed until the calculated peak striker force and the corresponding displacements match the experimental values. The stress distributions along the tensile face of the plate are then computed.

RESULTS AND DISCUSSION

A typical oscilliscope trace is shown in Figure 2, the large pulse indicating the instant at which the photographic mechanism is triggered. Oscillations of the striker-plate combination are superimposed on the trace. The initial peak is due to inertia effects and is indicative of the impulsive force required to accelerate the specimen to the striker velocity. Photographs are taken at various predetermined times and it is seen that there is no visual damage until the peak load is attained. A central crack then initiates and radial cracks propagate towards and beyond the supports. Figure 3 shows photographs obtained prior to and at the peak load. The available energy is considerably in excess of that required for crack initiation and further cracking occurs virtually instantaneously on attaining the peak force; the plate is broken into several pieces, usually four.

In simple plate theory, which is valid when the deflection is small in comparison with the plate thickness, stresses are independent of the elastic modulus. This assumption does not generally hold for these experiments and it is found that a change in modulus at constant load produces a change, albeit a comparatively small one, in the computed stresses. Initially, the modulus is assumed in the finite element analysis and the central deflection at the peak force is computed. An iterative approach is adopted, the modulus being adjusted until the calculated displacement matches the experimental one. Average peak values are used in the computation of load-striker displacement curves, which are shown in Figure 4. There is a slight increase in stiffness with increasing displacement of the smallest specimen, but nevertheless it is possible to make a reasonable linear approximation to the curve. In the other two specimens there is a clear departure from linearity, the stiffness increasing with increasing deflection as membrane stresses are introduced. The area under each curve yields the stored energy at fracture. This is not the same in the three cases, the largest specimen having about four times as much energy as the smallest, so it is clear that the fracture criterion is not a stored energy one.

The estimation of forces from underlying force–time curves is illustrated in Figure 5. The inertia peak is ignored and emphasis is placed on the portion of the curve just before the damage initiation peak. A linear approximation is used for the 60 mm square samples, but in other cases the estimation is based on force–time curves derived from the computed force–displacement curves. Clearly, a change in the force estimate changes the force–displacement curve, but Figures 4 and 5 are mutually consistent.

The final stage in the finite element analysis, after estimating the required force and the elastic modulus, is the computation of stresses. The distributions of circumferential and radial stress along the

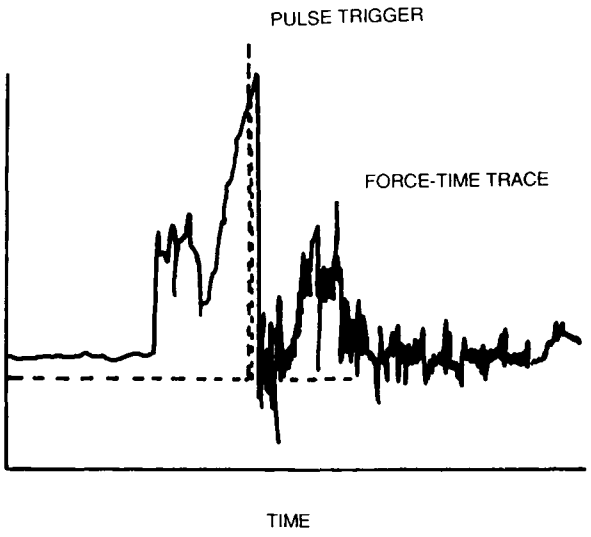

Figure 2 Storage oscilliscope trace.

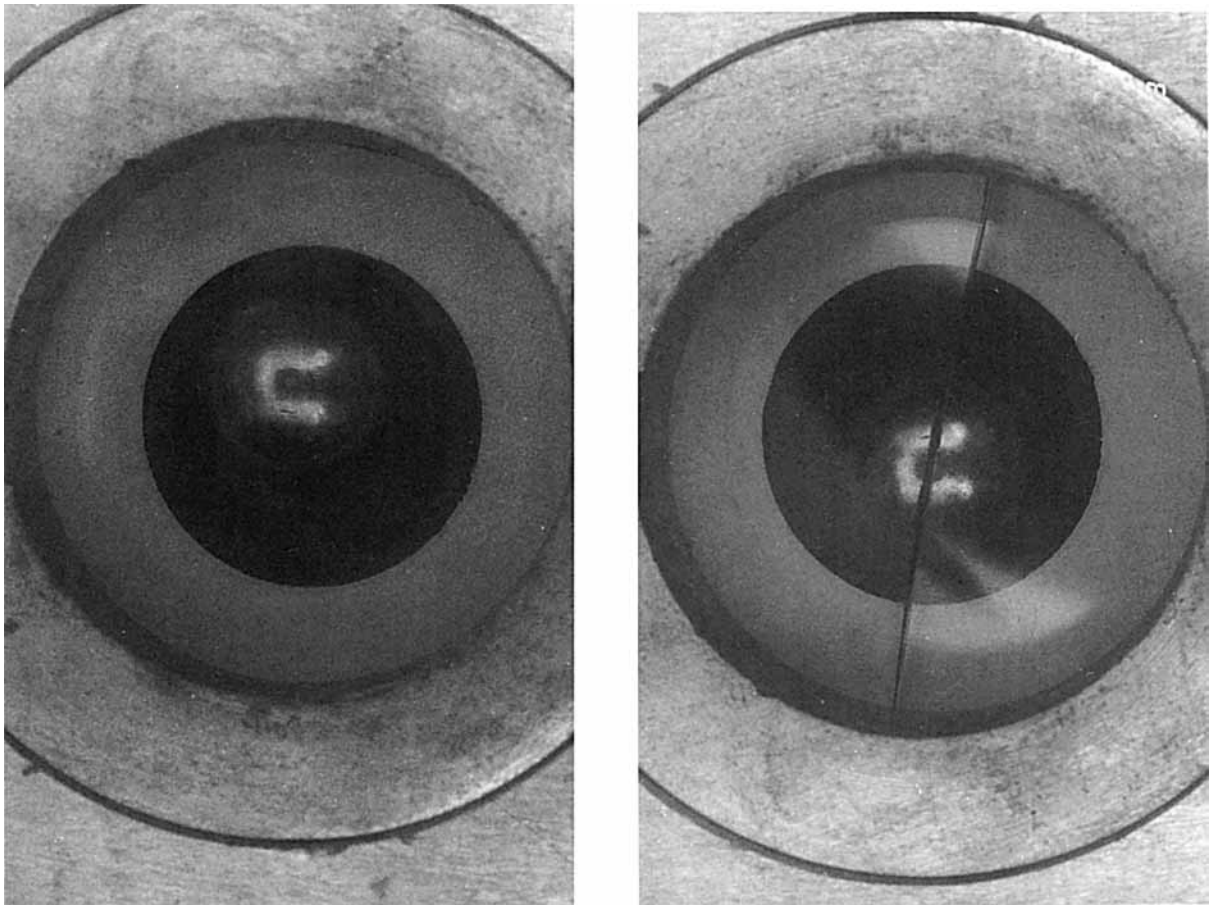

Figure 3 Photographs showing (left) the damage-free specimen prior to the peak load and (right) cracking at the peak load.

lower surfaces of the 60 mm square specimen, from the plate center to the support, is shown in Figure 6. The maximum stress occurs, as anticipated, at the center of the plate where there is a state of equibiaxial tension. Elsewhere, the circumferential stress is the greater one, thus accounting for the observation that after initiation at the center, cracks propagate radially, that is, normal to the circumferential direction. It is noted that there is a small radial compressive stress at the support, although the stress components are generally tensile. Figure 6 is based on a linear–elastic force-displacement relationship and the results may therefore be compared with those given by the linear–elastic stress analysis.[1] The outermost finite element node in contact with the striker is at a radius of 1.132 mm and this is taken as the radius of the contact zone. The Hookean analysis predicts a constant stress, the radial and circumferential stresses being equal, in the zone, the value depending on the selected zone radius size. If 1.132 mm radius is assumed as found using finite elements, then the calculated constant stress is 146.1 MPa. Outside this zone, the two stress distributions are similar to those derived using the finite element technique. The stress analysis based on simple plate theory is useful for giving a rapid indication of stress distributions, but finite elements facilitate the computation of stresses in the critical central region of contact where cracking initiates.

The finite element method has a further advantage in that it may be used in cases where membrane stresses are present. This includes the other two plates, for which the stress distributions are plotted in Figures 7 and 8. Comparing the three figures, it is seen that there is always a sharp decrease in stress, in the central region, with increase in distance from the center of the plate. Differences between the radial and circumferential stresses at any particular radius vary with the size of the support ring. When the support diameter is increased, the difference be-

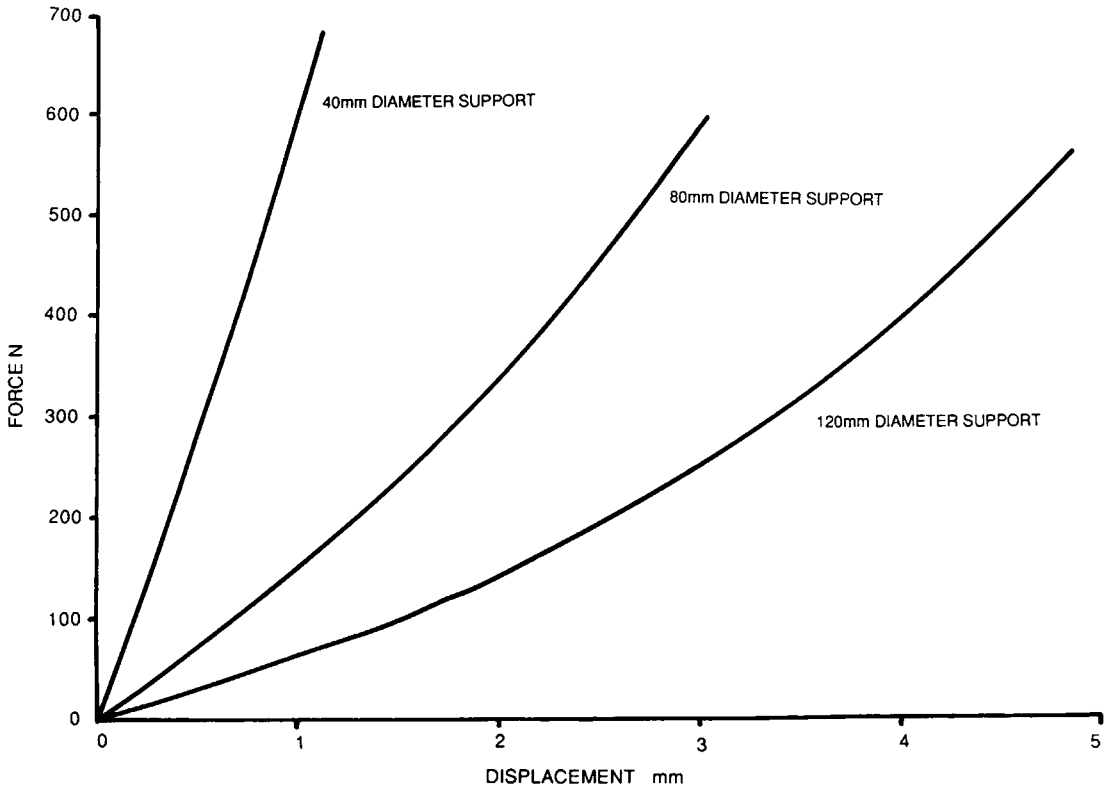

Figure 4 Computed force–displacement curves.

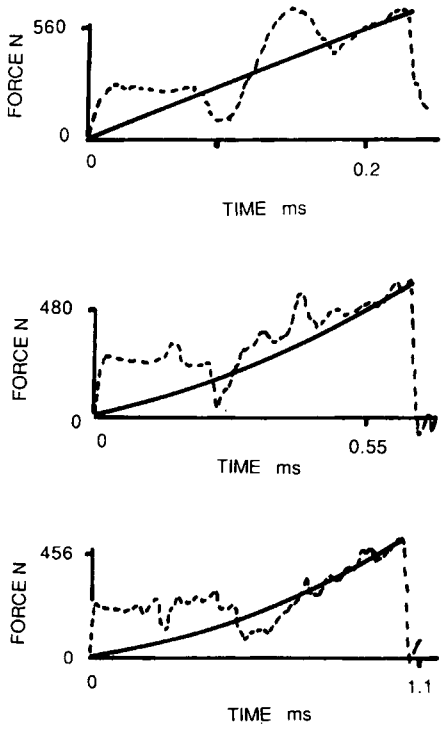

Figure 5 Force–time curves with peak force estimation for 60 mm (top), 100 mm (center), and 140 mm (bottom) square plates.

tween the circumferential and the radial stress in corresponding positions is reduced and there is a reduction in the circumferential stress at the support. The stress distributions are consistent with observations of crack initiation under the nose of the striker, followed by radial crack propagation under the action of the larger circumferential stress. Initiation is governed by the maximum stresses, the values of which are included in Table I, which shows the main experimental and computed results.

The maximum tabulated tensile stresses, which occur under the striker at the center, are approximately constant for the three support rings, thus indicating that failure occurs when this stress reaches a critical value. The stresses are substantially greater than the static strength. The rate-sensitivity of PMMA is illustrated by the work of Cheng et al.,[3] who measured tensile strengths over a range of rates and temperatures. At 24°C, the ultimate tensile strength increased from 71.5 MPa at a loading rate of 11.8 Ns^{-1} to 90.7 MPa at a rate of 777.5 Ns^{-1}. The respective strain rates are 1.67×10^{-6} s^{-1} and 1.67×10^{-4} s^{-1}. A good fit to the data was obtained using an expression for tensile strength as a function of absolute temperature, T, and loading rate, R. The final term, which becomes the dominant

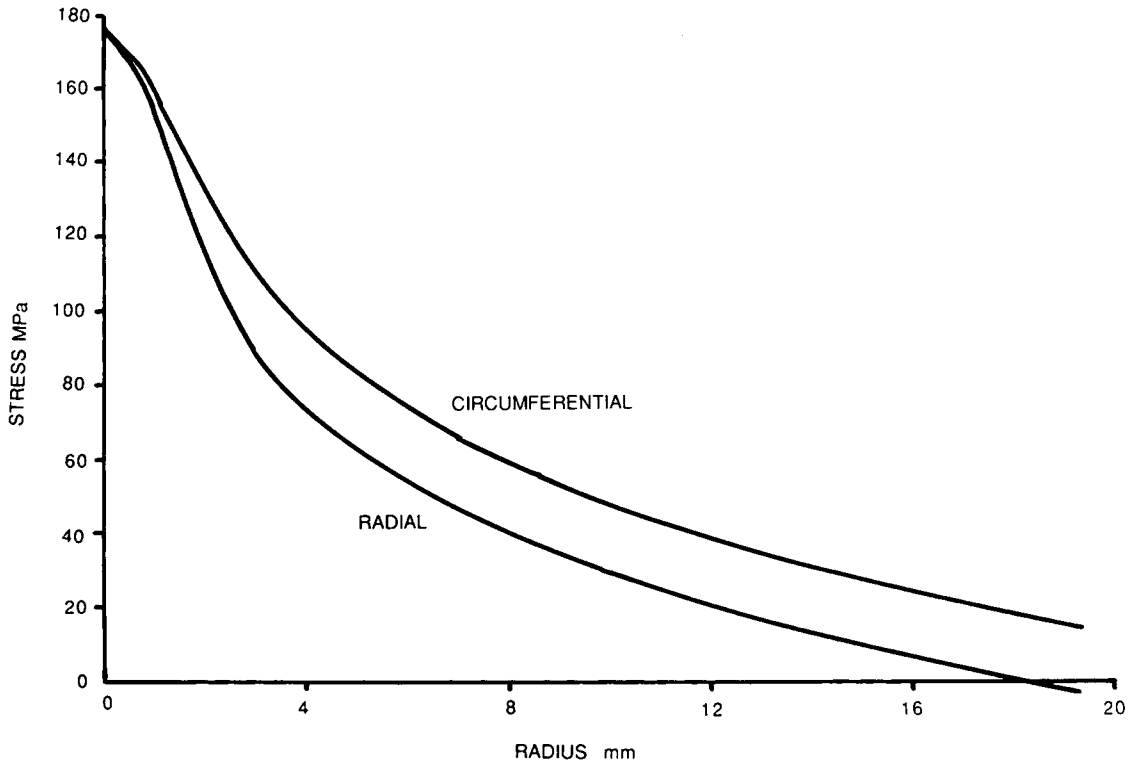

Figure 6 Circumferential and radial stress distributions for a plate supported on a 20 mm radius ring.

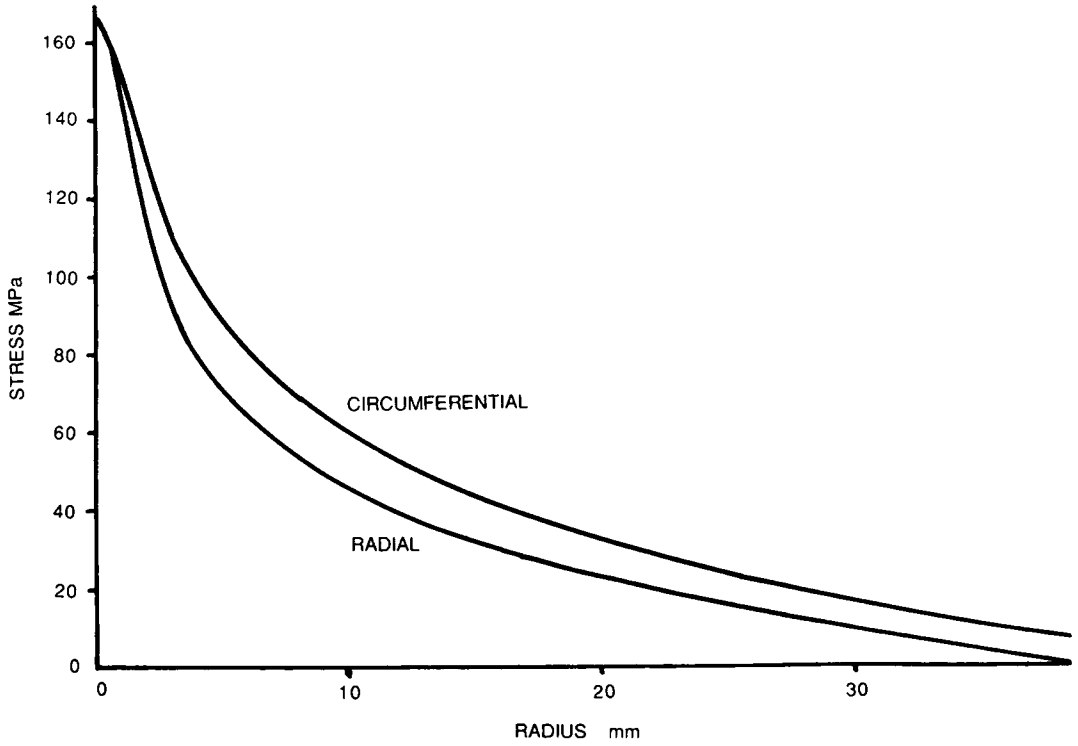

Figure 7 Stress distributions for a plate on a 40 mm radius support ring.

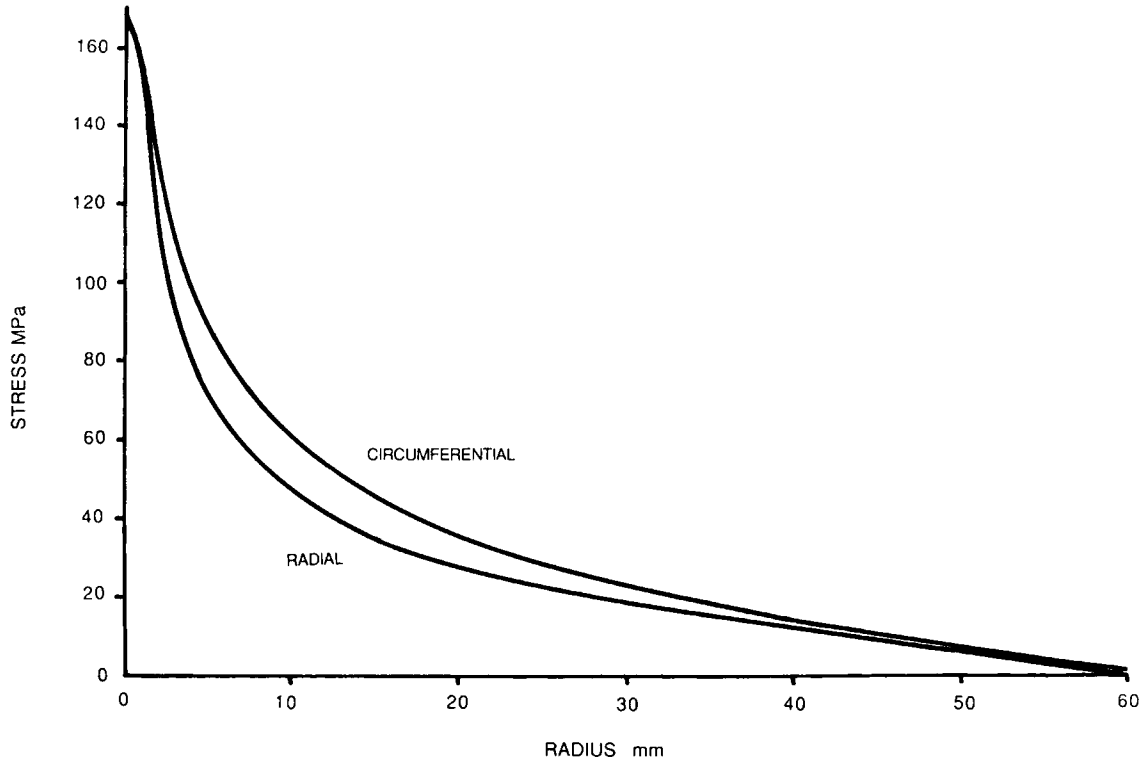

Figure 8 Stress distributions for a plate on a 60 mm radius support ring.

one at high rates, is 4.47 $\left(\frac{R}{T}\right)$ MPa, where R is in Ns^{-1} and T is in °K. The expression cannot be used at impact rates since the calculated stresses, at the test temperature and loading rates, are in excess of the modulus of elasticity, for example, 4.67 GPa at the slowest rate of the impact tests.

Extrapolation of the results[3] in terms of strain rate gives a more reasonable estimate of 144.9 MPa at the average rate of the impact experiments. This calculation involves extrapolation over many decades of strain rate and a further estimate has been made, involving extrapolation over less than a decade. Fleck et al.[4] have used a split Hopkinson tor-

Table I Experimental and Analytical Results

	Plate Length		
	60 mm	100 mm	140 mm
Experimental			
Available energy (J)	189.7	189.7	189.7
Peak Force (N)	680.7	593.6	555.4
Striker displacement at peak load (mm)	1.124	3.046	4.858
Impact energy (J)	0.383	1.024	1.656
Loading time (μs)	241	646	1020
Initial loading rate (Ns^{-1})	2.824×10^6	0.672×10^6	0.301×10^6
Computed			
Maximum tensile strength (MPa)	177.0	168.5	170.0
Elastic Modulus (GPa)	4.18	3.91	4.15
Local equivalent strain rate at crack initiation (s^{-1})	123.33	57.79	42.22

sion bar for shear strain rates from 500 s^{-1} to 2200 s^{-1}. Converting direct stresses and strains rates to equivalent shear values, the fracture stress obtained from an Eyring fit to the data is 172.4 MPa at the mean rate of the impact tests. This is in excellent agreement with the computed values, but the latter are probably overestimates, since the stress at fracture is pressure dependent[5] and the application of equibiaxial tension, with a positive dilational stress component, reduces the fracture stress.

The range of loading rates in the impact tests is relatively small, but the results exhibit rate-dependence to the extent that the maximum stress occurs at the greatest loading rate. Further interpretation of this effect is complicated by experimental scatter and the difficulty in estimating the peak load. This is illustrated by the facts that the maximum stress in the 60 mm square plates is greater than expected, relative to the other two plates, and that the computed maximum stress in the 140 mm plate, corresponding to the slowest loading rate, is greater than that in the 100 mm sample. It should be noted that the estimated modulus of elasticity of the 100 mm plaques is low and this leads to an underestimate of the maximum stress.

These elastic moduli adopted for computation to give satisfactory fitting to the experimental force–deflection curve are also significantly higher than the values at low rates. These calculated moduli are in the same ranking order as the maximum stresses, although there is little difference between the values for the 60 mm and the 140 mm square plates. They are affected by any errors in determination of the peak load. It is relatively easy to estimate the time and displacement at this load and a change in the estimated load will produce a change in the computed modulus to maintain the same deflection at a different load. The average modulus is 4.08 GPa, which appears to be reasonable in comparison with other quoted values. Adams et al.[6] obtained a value of 3.7 GPa from the striker stiffness in notched impact tests conducted at the relatively low striker velocity of 0.5 m/s. Cheng et al.[3] estimated elastic moduli from energy release rates of notched three-point bending specimens. The room temperature value is slightly over 4 GPa at a loading rate of 22000 Ns^{-1}. Döll and Könczöl[7] have presented creep moduli, obtained in various tests, as a function of loading time. The value for dynamic tests at the average loading time of the impact tests is about 4.2 GPa.

It will be necessary to test other materials in order to determine if the proposed criterion, of failure on reaching a critical tensile stress, is generally applicable. In ductile polymers, it is anticipated that the stress at fracture initiation is the von Mises effective stress. In the plate–specimen, the stress at the center is, as previously stated, equibiaxial tension and the maximum stress is the same as the equivalent stress. Any pressure dependence at yield will not be apparent unless the stress state is changed. It is not possible to distinguish between the two criteria, the maximum stress one being preferred in this case, because the fracture is brittle.

It is concluded that the results of these impact tests exhibit rate dependence, both in comparison with static values and, to a lesser extent, within the comparatively small range of loading times of the experiment. Brittle fracture of this material occurs when the maximum tensile stress attains a (time-dependent) critical value.

The financial support of the Science and Engineering Research Council (Grant Number GR/F04346. Failure Criteria for Impact Damage in Moulded Plastics) is gratefully acknowledged.

REFERENCES

1. P. E. Reed, *J. Strain Anal.*, **25,** 207 (1990).
2. R. P. Nimmer, *Polym. Eng. Sci.*, **23,** 155 (1983).
3. W. M. Cheng, G. A. Miller, J. A. Manson, R. W. Hertzberg, and L. A. Sperling, *J. Mater. Sci.*, **25,** 1917 (1990).
4. N. A. Fleck, W. J. Stronge, and J. H. Liu, *Proc. R. Soc. Lond. A*, **429,** 459 (1990).
5. K. Matsushige, E. Baer, and S. V. Radcliffe, *J. Polym. Sci. Polym. Phys. Ed.*, **14,** 703 (1976).
6. G. C. Adams, R. C. Bender, B. A. Crouch, and J. G. Williams, *Polym. Eng. Sci.*, **30,** 241 (1990).
7. W. Döll and L. Könczöl, in *Advances in Polymer Science 91/92,* H. H. Kausch, Ed., Springer, Berlin, 1990.

Received August 5, 1991
Accepted January 20, 1992